JGR Space Physics

RESEARCH ARTICLE
10.1029/2020JA029094

**Key Points:**

- Quasi 10-day and quasi 6-day waves (Q6DW) were observed in the mesospheric winds from the Antarctic and tropical meteor radars during the 2019 Southern Hemisphere (SH) sudden stratospheric warming (SSW)
- The Q6DW were also detected in the geopotential height measurements from the Microwave Limb Sounder over the northern tropical station
- The Whole Atmosphere Community Climate Model simulation constrained only up to 60 km illucidates that the Q6DW originated from the high-latitude mesosphere in SH during SSW

**Correspondence to:**
Y. H. Kim,
yhkim@cnu.ac.kr

**Citation:**
Lee, W., Song, I.-S., Kim, J.-H., Kim, Y. H., Jeong, S.-H., Eswaraiah, S., & Murphy, D. J. (2021). The observation and SD-WACCM simulation of planetary wave activity in the middle atmosphere during the 2019 Southern Hemispheric sudden stratospheric warming. *Journal of Geophysical Research: Space Physics*, *126*, e2020JA029094. https://doi.org/10.1029/2020JA029094

Received 30 DEC 2020
Accepted 11 MAY 2021



# The Observation and SD-WACCM Simulation of Planetary Wave Activity in the Middle Atmosphere During the 2019 Southern Hemispheric Sudden Stratospheric Warming

**Wonseok Lee[1], In-Sun Song[2], Jeong-Han Kim[2], Yong Ha Kim[1], Se-Heon Jeong[1,3], S. Eswaraiah[1], and D. J. Murphy[4]**

[1]Department of Astronomy, Space Science, and Geology, Chungnam National University, Daejeon, South Korea, [2]Yonsei University, Seoul, South Korea, [3]Korea Astronomy and Space Science Institute, Daejeon, South Korea, [4]Australian Antarctic Division, Kingston, TAS, Australia

**Abstract** A sudden stratospheric warming (SSW) is an extremely rare event in the Southern Hemisphere (SH), but occurred in early September 2019. From the Antarctic meteor radar (MR) stations, Davis (68.6°S, 77.9°E) and King Sejong Station (62.2°S, 58.8°W), quasi 10-day oscillations were clearly observed in the zonal mesospheric winds before the central date (DOY 253) of the SSW. From the northern low-latitude Tirupati (13.6°N, 79.4°E) MR, a strong wave activity with a period of ~6 days was detected in the zonal winds right after the central date. This oscillation is also seen in the geopotential height measurements from the Microwave Limb Sounder (MLS) on board the Aura satellite near the Tirupati region. To elucidate the possible source of the quasi 6-day wave (Q6DW), we use a specified dynamics version of the Whole Atmosphere Community Climate Model (SD-WACCM) constrained by the reanalysis data from the surface to 50 km. The simulation results show that the amplitude of the westward and equatorward propagating Q6DW was enhanced after the SSW central date in the MLT region, and the Q6DW can be attributed to the baroclinic/barotropic instability in the SH high-latitude mesosphere where the divergence of Eliassen-Palm flux occurred. Thus, we suggest that the Q6DW activity observed by the Tirupati MR and MLS originated from the SH high-latitude mesospheric region. Both the observation and the simulation results clearly demonstrate that the 2019 SH SSW affected not only the high-latitude MLT region but also the low-latitude MLT region.

**Plain Language Summary** A sudden stratospheric warming (SSW) is an extremely rare event in the Southern Hemisphere (SH) but occurred in early September 2019. We report the planetary wave activity (~10-day and ~6-day periods) in the mesospheric winds measured by Antarctica and tropical meteor radars during the SSW. The 6-day wave has also been reported in the equatorial electrojet measurements by satellites. The observed planetary wave activity was successfully simulated by a theoretical global circulation model constrained by reanalysis data only up to the stratospheric altitude. The simulation identifies the source of the waves at the high latitude of the Southern Hemisphere and the propagation to the tropical region during the SSW.

## 1. Introduction

The climatological zonal mean zonal wind in the winter stratosphere is normally eastward, and the climatological zonal mean temperature decreases poleward in the winter high-latitude regions (Andrews et al., 1987). However, when a sudden stratospheric warming (SSW) occurs, the stratospheric temperature dramatically increases in the polar region by 40–60 K in a week, leading to the reversal of the meridional temperature gradient and a weak or reversed polar jet in the stratosphere (e.g., Andrews et al., 1987; Eswaraiah et al., 2017, 2020; Krüger et al., 2005; Newman & Nash, 2005; Pancheva et al., 2008). The SSW has been understood traditionally as the interaction between the strong upward propagating planetary waves (PWs) and mean flow in the winter hemisphere (Matsuno, 1971), but it should be noted that various studies have emphasized the importance of gravity wave processes other than PWs in the occurrence of the SSW (see Song et al., 2020 and references therein). According to the World Meteorological Organization (WMO), the SSW can be classified as a major warming when the meridional gradient of zonal mean temperatures is reversed in the polar stratosphere and the reversal of eastward zonal mean zonal winds occurs. In case

of the reversal of the meridional temperature gradient without wind reversal, the SSW event is called a minor warming. Although the occurrence of an SSW event is usually determined by the zonally averaged quantities, the SSW is a dynamical process essentially characterized by longitudinal asymmetry (Andrews et al., 1987; Hoffmann et al., 2007; Matthias et al., 2013).

The SSW is basically a phenomenon in the winter stratosphere, but it can affect the upper atmosphere not only in the polar regions but also in the tropical regions (Pedatella et al., 2018). The first report of SSW effects on the tropical mesosphere and lower thermosphere (MLT) region was presented by Fritz and Soules (1970) using a satellite infrared spectrometer. More recently, there have been a great deal of studies about dynamical changes and variation of PWs amplitude in the tropical MLT region related to northern SSWs (e.g., Chandran & Collins, 2014; Gan et al., 2020; Koushik et al., 2018; Sathishkumar & Sridharan, 2009; Shepherd et al., 2007; Vineeth et al., 2009)

SSW occurrence in the Southern Hemisphere (SH) is very rare compared to counterparts in the Northern Hemisphere (NH). This is thought to be due to the typically larger amplitude of stationary PWs in the NH, where planetary-scale orographic forcing is strong (e.g., Andrews et al., 1987). Only one major SH SSW, in 2002, was reported thus far, with a few minor SSWs, including the one in 2010 and the recent 2019 warmings (e.g., Dowdy et al., 2004; Eswaraiah et al., 2016, 2020; Yamazaki et al., 2020). Newman and Nash (2005) reported using reanalysis data that strong PWs were observed in the SH mid-latitude lower troposphere and propagated to the polar stratosphere, resulting in the first observed 2002 major SH SSW. Both the ground-based and space-borne instruments observed mesospheric cooling in the Antarctic region during the 2002 major SSW (Azeem et al., 2005; Hernandez, 2003; Siskind et al., 2005). Dowdy et al. (2004) showed that the mesospheric zonal wind was reversed about a week before the reversal of the stratospheric zonal wind during the 2002 SH SSW. Mbatha et al. (2010) also found that the reversal of the MLT zonal wind preceded the reversal at 10 hPa by using the HF radar and reanalysis data during the 2002 SH SSW. It has been reported that both the 2002 major and the 2010 minor SH SSW affected the mesospheric dynamics and temperature as NH SSWs can. Eswaraiah et al. (2016, 2017) found, using the meteor radar and a model simulation, that even the minor 2010 SH SSW affected the mesospheric temperature cooling in the Antarctic region. Furthermore, strong PW activity and amplified tides were observed in the SH mesospheric region by MF radar (Dowdy et al., 2004, 2007) airglow measurements (Azeem et al., 2005, 2010), temperature observations from a satellite (Palo et al., 2005), numerical models (Chang et al., 2009), and meteor radar (Eswaraiah et al., 2016, 2018).

Only a small number of studies have focused on the response of the SH SSW on the tropical MLT regions, which is probably due to its rare occurrence. Guharay et al. (2014) investigated the effects of the major 2002 SH SSW on extra-tropical latitudes with wind and temperature observations in Cachoeira Paulista (22.7°S, 45.0°W). They found a temperature cooling in the tropical stratosphere corresponding to the polar stratospheric warming. The equatorward propagation of the PWs with zonal wavenumbers 1 and 2 was also found in the stratosphere, but no PW activity was detected in the mesosphere during the SSW event. For tides, significant diurnal and semidiurnal tidal responses were found in the middle atmosphere prior to the 2002 SH SSW from reanalysis data and the same meteor radar observations at Cachoeira Paulista (Guharay & Batista, 2019). Bhagavathiammal et al. (2016) compared the dynamical responses to the 2009 NH major SSW and 2002 SH major SSW in the low-latitude region using the mesospheric wind data. They found that the strong PW energy propagated from high- to low-latitudes during both the major events, although the 2009 one reached further into lower latitudes than the 2002 one.

In early September 2019, an SSW occurred in the SH (Eswaraiah et al., 2020; Goncharenko et al., 2020; Miyoshi & Yamazaki, 2020; Yamazaki et al., 2020). During the 2019 SH SSW, the polar stratospheric temperature (90°S and 10 hPa) increased by about 50 K per week from 5 to 11 September; the rate of increase is the largest in the entire Modern-Era Retrospective analysis for Research and Applications, Version 2 (MERRA-2) data set. Eswaraiah et al. (2020) noted that the polar-mesospheric zonal winds were reversed for about 20 days before the 2019 SSW and also observed the signature of PWs before and after the SSW. Yamazaki et al. (2020) detected the quasi 6-day wave (Q6DW) in the tropical MLT regions using the geopotential heights retrieved from measurements by the Earth Observing System Microwave Limb Sounder (MLS) on board the Aura satellite. In addition, the Q6DW also appeared in the equatorial ionospheric data from the European Space Agency's (ESA) Swarm satellites. Yamazaki et al. (2020) focused on the effects

**Table 1**
*Operational Parameters of Three Meteor Radars*

| | Davis (68.6°S, 77.9°E) | King Sejong station (62.2°S, 58.8°W) | Tirupati (13.6°N, 79.4°E) |
|---|---|---|---|
| Frequency | 33.2 MHz | 33.2 MHz | 35.2 MHz |
| Power | 6.8 kW | 12 kW | 40 kW |
| PRF | 430 Hz | 440 Hz | 430 Hz |
| Duty cycle | 8.3% | 8.4% | 12% |
| Reference | Holdsworth et al. (2008) | Kim et al. (2010) | Rao et al. (2014) |

of the 2019 SH SSW on the equatorial ionospheric region without analyzing in detail the origin and propagation characteristics of the Q6DW. Given the extreme state of the SH polar stratosphere during the early spring of 2019 due to the SSW, it is expected that the SH SSW can affect the upper atmosphere not only at the high latitudes but also at the low latitudes.

In this paper, we examine the observational features of the dynamics and PW activity in the upper atmosphere response to the 2019 SH SSW in the high- and low-latitudes by using data from meteor radars (MRs), satellite (MLS), and the MERRA-2 reanalysis data. In addition, we attempt to identify the source of the observed Q6DW by using the specified dynamics version of the Whole Atmosphere Community Climate Model (SD-WACCM). In Section 2, the data set used in this study is described. Sections 3.1–3.3 presents the analysis results for the characteristics of the 2019 SH SSW. Section 3.4 contains observational analysis of PW activities. The analysis of the source for the Q6DW is carried out in Section 3.5. Finally, a summary and conclusion are presented in Section 4.

## 2. Data

### 2.1. Meteor Radars

In this study, we used three MRs located at Davis (68.6°S, 77.9°E), King Sejong Station (KSS; 62.2°S, 58.8°W), and Tirupati (TP; 13.6°N, 79.4°E). The MRs routinely derive hourly horizontal winds from measured meteor trail echoes in the MLT region (~70–~100 km altitude) with 2 km height bins. The three MRs allow us to study the latitudinal difference of horizontal winds and PW activity between the tropical region and high-latitude region during the SSW event. In addition, the longitudinal asymmetry of the high-latitude MLT dynamics can be investigated by comparing data from the Davis MR and KSS MR.

The Davis MR operates at a frequency of 33.2 MHz with a peak power of 6.8 kW. The transmitter has a maximum duty cycle of 8.3% with a 430 Hz Pulse Repetition Frequency (PRF) (Holdsworth et al., 2008). The KSS MR, installed in March 2007, also operates at a frequency of 33.2 MHz, with a duty cycle of 8.4% and a 440 Hz PRF (Kim et al., 2010). The transmitter power was upgraded to 12 kW in 2012, increasing detection counts to about 15,000–40,000 meteor echoes a day. The TP MR using 35.2 MHz frequency was more recently installed, in August 2013, and has been detecting an average count of 40,000 meteor echoes per day with a high transmitter power (40 kW) and a duty cycle of up to 12% (Rao et al., 2014). The operation parameters of MRs are summarized in Table 1.

### 2.2. Aura/MLS

Atmospheric temperatures and geopotential heights (GPHs) retrieved from observations provided by the Earth Observing System (EOS) MLS on board the Aura satellite (Schwartz et al., 2008). The NASA (National Aeronautics and Space Administration) Aura satellite was launched in July 2004 and has been operating in a sun-synchronous orbit at an altitude of 705 km. In this study, the EOS MLS version 4.2x level 2 data are employed. The validated vertical range of the MLS temperatures and GPHs data is from 261 to 0.001 hPa. For this pressure range, the data with a quality greater than 0.2 and convergence less than 1.03 are only used to ensure reasonable data quality (see the v4.2x data quality document [Livesey et al., 2018] for details on data retrieval and quality control). Geometric heights ($z$) of temperature measurements are derived from

the GPH ($z_g$) using the equation $z = z_g R_e(\phi)\left[R_e(\phi) - z_g\right]^{-1}$, where $R_e(\phi)$ is the Earth's radius at the latitude of $\phi$ based on the WGS84 ellipsoid model (Younger et al., 2014). The global distribution of temperatures and GPHs is produced using the daily mean measurements in the 5° × 20° latitude and longitude grids. Daily mean temperatures and GPHs at the location of MRs are derived from the data of a 5° × 20° latitude and longitude bin whose center is the MR location.

### 2.3. MERRA-2

The MERRA-2 reanalysis data set (Gelaro et al., 2017) is used for the overview of 2019 SH SSW. The data set provides temperatures, horizontal winds, and GPHs in the 0.5° × 0.625° latitude and longitude grids and 72 vertical levels (model level data set) from the surface to 0.01 hPa (~80 km). Zonal winds and GPHs from MERRA-2 are used to examine the zonal mean zonal wind reversal and PW activity at 60°S, respectively.

### 2.4. SD-WACCM

To elucidate the possible source of PWs, we utilize the specified dynamics (SD) version of WACCM6 (Gettelman et al., 2019). WACCM6 is the mesospheric and lower-thermospheric extension (up to ~140 km) of the Community Atmosphere Model version 6 (CAM6). The CAM6 or WACCM6 can be used as a component model for the atmosphere in the Community Earth System Model version 2 (CESM2; Danabasoglu et al., 2020) developed at the National Center for Atmospheric Research (NCAR). WACCM6 includes almost the same physical processes as CAM6 except that WACCM6 additionally contains the nonorographic gravity wave drag parameterization, solar and geomagnetic forcing, and gas and aerosol chemistry (see Gettelman et al., 2019 for details).

In this study, we carried out an SD experiment for the 1.9° × 2.5° horizontal resolution using WACCM6 for a period from 1 January 2018 to 15 December 2019. WACCM6 is coupled with interactive chemistry. In this experiment, the middle atmosphere (MA) scheme with the D-region chemistry (see Gettelman et al., 2019) is used. For the SD run, horizontal winds and temperature, surface pressure, surface stress and heat fluxes in WACCM6 are relaxed toward the linearly time-interpolated 3 hourly MERRA-2 reanalysis. The relaxation coefficient is uniform below $z = 50$ km, linearly decreases with height above 50 km, and it becomes zero above 60 km as described by Brakebusch et al. (2013). Therefore, the model is unconstrained by reanalysis above 60 km.

The default horizontal resolution of WACCM6 is 0.95° × 1.25°, but the experiment in this study is performed at the 1.9° × 2.5° resolution. For this low-resolution run, a model initial condition for January 1 is produced using balanced dynamical variables (horizontal winds, temperature, and surface pressure) from an existing low-resolution initial condition for WACCM4 and horizontally interpolated constituent variables required for the higher-resolution WACCM6. The use of the dynamically balanced variables from a WACCM4's initial condition helps reduce the model spin-up time. The auxiliary data required for the SD experiment (e.g., the sea surface temperature and sea-ice fraction, solar and geomagnetic indices, and the ionization rates due to energetic particle precipitation) are extended in time to include the simulation period. For the sea surface temperature and sea-ice, the extension is achieved by combining the NOAA Optimal Interpolation (OI) product (Reynolds et al., 2002) for the extended period with existing data made using the merging method (Hurrell et al., 2008). For the solar and geomagnetic indices, NASA GSFC Space Physics Data Facility (SPDF) OMNI hourly data (King & Papitashvilli, 2005) are used for the extension. For the ionization rate, the Chemistry-Climate Model Initiative (CCMI) Ref-C2 experiment data for future climate (Eyring et al., 2008, 2013) are used to extend the existing ionization rate for the period from 1963 to 2018.

## 3. Results and Discussion

### 3.1. Overall Characteristics of the 2019 SH SSW

Figure 1 shows the overall characteristics of the 2019 SH SSW using the MERRA-2 data. For comparison, the climatological mean and the 2002 major SSW data are included in each panel. The climatological mean is based on the period from 1980 to 2019, and the shaded areas represent the one standard deviation from

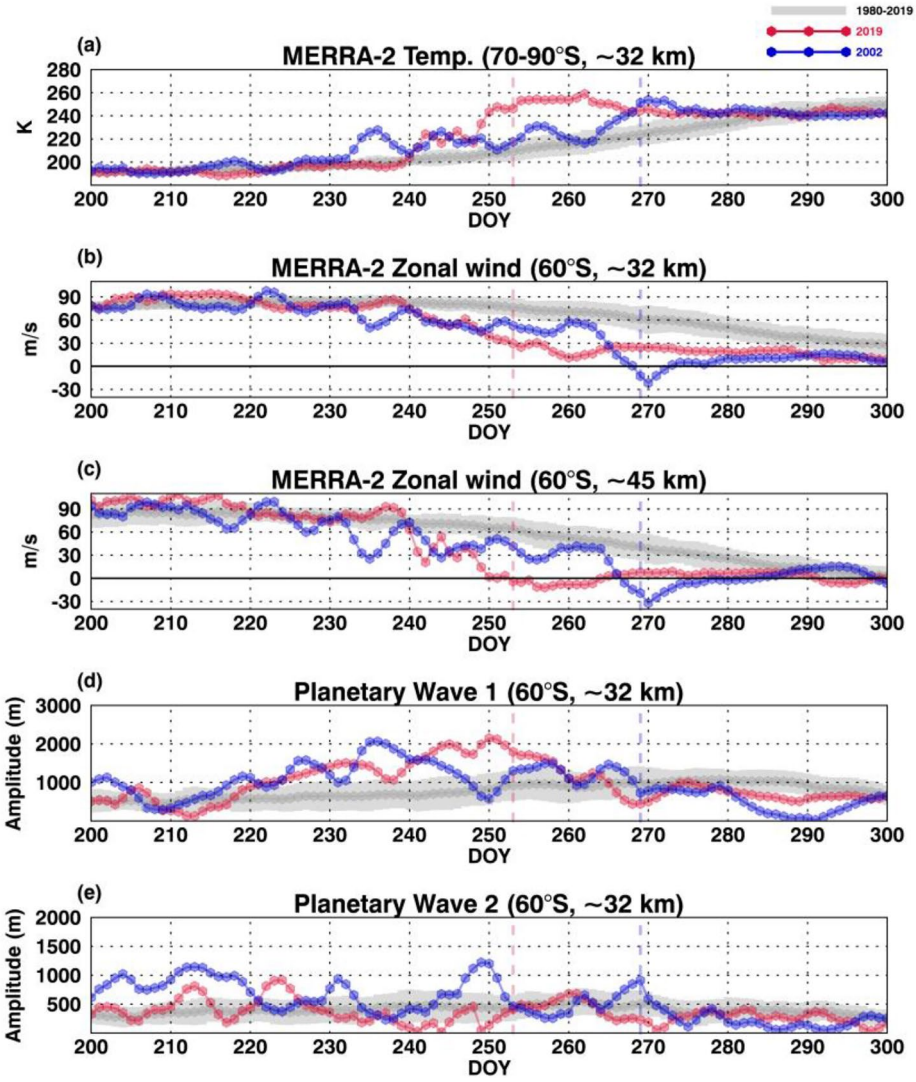


**Figure 1.** Overall characteristics of the 2019 Southern Hemisphere sudden stratospheric warming (SH SSW) using the MERRA-2 data: (a) The zonal-mean temperatures averaged over the polar region (70°S–90°S), (b and c) The zonal-mean zonal winds at 60°S at 32 km (10 hPa) and 45 km (1.5 hPa), respectively. (d and e) The amplitudes of PWs with zonal wavenumber 1 and 2 (PW1 and PW2), respectively, at ~32 km and 60°S. The climatological and 2002 major SSW data are overplotted in each panel. The climatological mean is obtained for the period of 1980–2019, and the shaded areas represent one standard deviation from the mean. The vertical dashed lines represent the central dates of the 2002 and 2019 SSW.

the mean. In Figure 1a, the zonal mean temperatures averaged over the polar region (70°S–90°S) at the 10 hPa (~32 km) rapidly increase from 204.3 K at DOY 240 (August 28) to 246.3 K at DOY 253 (September 10). The maximum variation in the temperatures averaged over the polar region is 37.0 K/week during the 2019 SSW, which is larger than 35.5 K/week in the 2002 major SSW. Yamazaki et al. (2020) also provide an overview of the 2019 SH SSW using the MERRA-2 temperatures at 90°S and 10 hPa. They noted that the polar temperature increase (at 90°S) in a week during the 2019 SSW is the largest (50.8 K/week) throughout the whole period (from January 1980 to the present) of the MERRA-2 data set.

The zonal-mean zonal winds at 32 and 45 km at 60°S are shown in Figures 1b and 1c. The zonal-mean zonal wind at 32 km started to deviate from the climatological values on DOY 239 in 2019, but there is no wind reversal as in 2002. However, a wind reversal occurred at the altitude of ~45 km around DOY 253 in 2019. Based on this reversal, we specified the central date of the 2019 SSW on DOY 253. According to the WMO's definition of an SSW, the 2019 SSW can be classified as a minor SSW, but the variation in temperatures

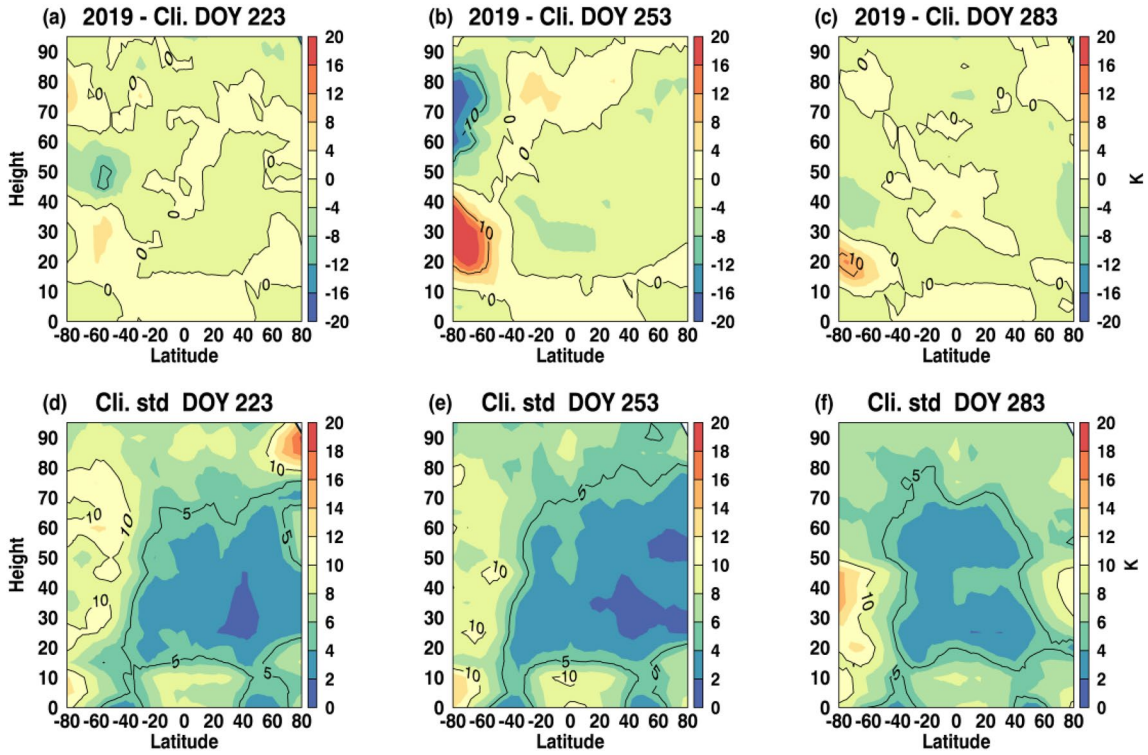


**Figure 2.** (a–c) Differences between the zonal-mean Aura/Microwave Limb Sounder temperature and the zonal-mean climatology and (d–f) the standard deviation of the zonal-mean temperature for non-SSW years 30 days (DOY 223) before the central date of the 2019 Southern Hemisphere sudden stratospheric warming (SH SSW), the central date (DOY 253), and 30 days (DOY 283) after the central date. Climatology data are obtained from the averages over the period from 2004 to 2018, except for 2010 when the minor SH SSWs occurred, respectively.

was unusually large, even stronger than the 2002 major SSW. Yamazaki et al. (2020) also categorized this event as a minor warming based on the zonal mean zonal winds at 60°S derived from the Aura/MLS GPH, which is similar to those from the MERRA-2 reanalysis, and the MERRA-2 polar stratospheric temperatures. Figures 1d and 1e show the amplitude of PWs (GPH perturbations) with zonal wavenumber 1 and 2 (PW1 and PW2), respectively, at ~32 km and 60°S. The amplitude of PW1 is substantially enhanced around DOY 253 when the zonal wind reversal occurred at 45 km and was larger than that before the central date (DOY 269; September 26) in the 2002 major SSW. Meanwhile, the amplitude of PW2 in 2019 is within the climatological variability. According to the traditional criteria for categorizing SSWs (Nakagawa & Yamazaki 2006), the 2019 SSW event is preferentially associated with PW1, similar to the 2002 SH major SSW (Krüger et al., 2005), and thus can be classified as a displacement-type minor SSW.

### 3.2. Global Temperature Observations From Aura/MLS

The effects of the 2019 SH SSW on the global atmospheric temperatures are investigated using Aura/MLS measurements. Figure 2 presents the zonal-mean temperature difference from the climatological mean on the SSW central date (DOY 253), and 30 days before (DOY 223) and after (DOY 283) the central date. Climatology data are obtained for the period of 2004–2018 (except for 2010 when the SH SSWs occurred). The variations of temperatures are clearly seen in the SH high-latitude stratosphere and mesosphere around the SSW central day. The maximum temperature increase (31.8 K) and decrease (−21.3 K) are found in the polar stratosphere and mesosphere regions, respectively, on the central date. The region with a temperature difference more than 10 K, which is much higher than the climatological standard deviations for non-SSW years (8–10 K; Figure 2e), seems to extend to ~60°S. These variations of temperatures during the 2019 SH SSW are comparable to the composite result for all NH major SSWs in the period between 1988 and 2010 made using SD-WACCM (Chandran & Collins, 2014). In the NH major SSW composite, a zonal mean temperature anomaly up to ~30 K occurs in both the stratosphere and mesosphere, as PW breaking and gravity

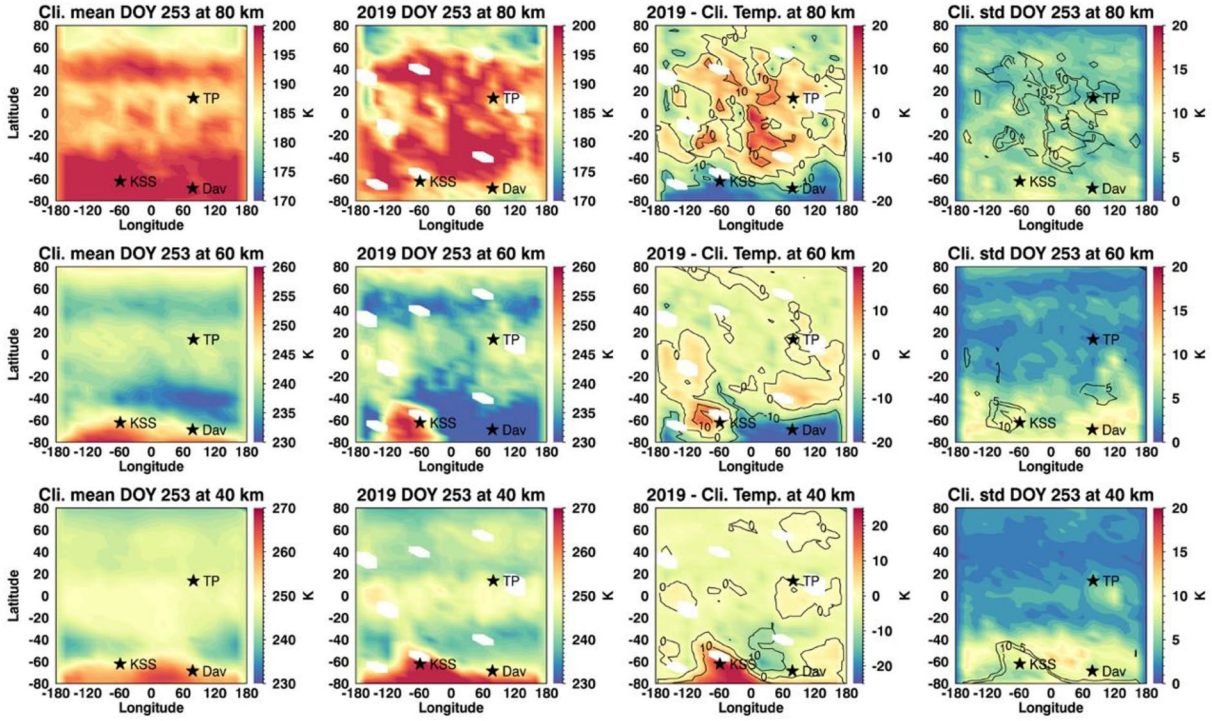


**Figure 3.** The horizontal distributions of (first column) the climatological mean Aura/Microwave Limb Sounder temperature, (second column) the temperature in 2019, (third column) the difference between the climatology and 2019 data, and (fourth column) the standard deviation from the climatological mean on DOY 253 for non-Southern Hemisphere sudden stratospheric warming (SH SSW) years at the altitude of (top) 80 km, (middle) 60 km, and (bottom) 40 km on the central date of the 2019 SH SSW. The locations of MRs are marked with a black asterisk.

wave forcing induce stratospheric warming and mesospheric cooling, respectively. After the central date of the 2019 SSW (DOY 283; Figure 2c), the high-latitude temperature anomaly returns to the normal state.

Figure 3 presents Aura/MLS temperature comparison with the climatological values during the 2019 SH SSW event at the altitude of 40, 60, and 80 km on the central date of the SSW. The first and second columns of Figure 3 show the temperature maps for the climatologic mean on DOY 253 and for the 2019 SSW, respectively. The third and fourth columns of Figure 3 display the temperature differences between the 2019 SSW and the climatological mean on DOY 253 and the standard deviation from the climatological mean obtained for non-SH SSW years, respectively.

Figure 3 clearly shows that the temperature increased in the vicinity of KSS with the maximum increase of 37.2 K from the climatological mean at the altitude of 40 km (see the bottom panel in the third column), whereas the temperature decreased from the climatologic mean near the Davis Station, indicating the displaced polar vortex toward KSS (Chandran & Collins, 2014). On DOY 253, the center of the displaced polar vortex was located over KSS in the low-to-middle stratosphere (Rao et al., 2020), and the vortex was being broken around the altitude of 40 km. At the altitude of 60 km, the temperature near the Davis Station remarkably decreased by about −34.2 K, while the temperature increased by about 15.4 K near the KSS station. At the altitude of 80 km, most of the high-latitude regions shows temperature cooling, and the longitudinal variation of the cooling is weak compared with the upper stratosphere. Based on the ground-based measurements, Hoffmann et al. (2007) noted that there are weak longitudinal variations of temperatures in the high-latitude mesopause region during northern major SSWs, which is similar to our findings in Figure 3 in the southern SSW.

In the tropical region, there is a temperature increase of more than 10 K at the altitude of 80 km in the longitude range of 0°–40°E during the 2019 SH SSW, with the maximum increase of 22.6 K near the equator. However, the temperature anomaly around the TP station is not significant as it falls within the standard deviation from the climatological mean. Sridharan et al. (2010) observed the mesospheric warming during

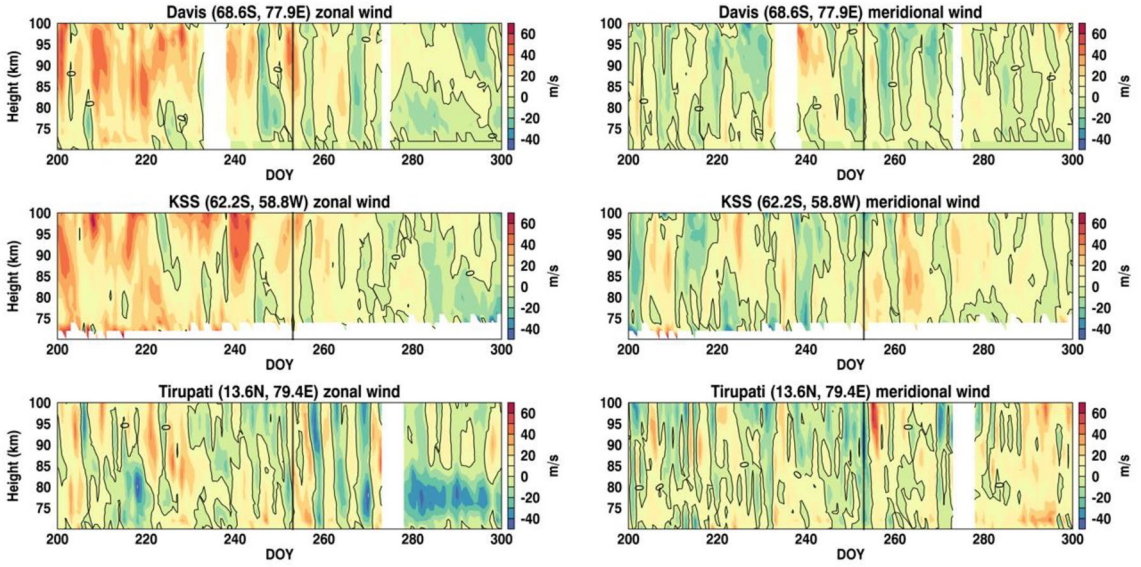


**Figure 4.** The daily zonal (left) and meridional (right) winds from Davis (top), King Sejong Station (middle), and TP (bottom) meteor radars in the altitude range of 70–100 km. The central date of the 2019 Southern Hemisphere sudden stratospheric warming is denoted by the black vertical lines.

the 2009 northern hemispheric SSW using a Rayleigh lidar and satellite measurements at Gadanki (13.5°N, 79.2°E) and found temperature increases of 10–15 K in the altitude range between 70 and 80 km in the equatorial region. Mesospheric warming during the SSW event in the tropical region is mainly related to the change of meridional circulation associated with the SSW. Laskar et al. (2019) noted from the Navy Global Environmental Model (NAVGEM) High Altitude (NAVGEM-HA) that the zonal-mean southward wind extended over the entire NH during the 2010 and 2013 NH major SSW events. According to the change of meridional circulation, a downward flow can be produced in the equatorial mesosphere, causing an increase in temperature (Miyoshi et al., 2015).

The present temperature observations from Aura/MLS on the central date of the 2019 SSW can be summarized as follows: (a) a zonal-mean temperature increases and decreases in the high-latitude stratosphere and mesosphere with maxima of 31.8 K and −21.3 K, respectively; (b) a longitudinal asymmetry in the high-latitude stratosphere but almost nonexistence of the asymmetry in the high-latitude mesosphere; and (c) a temperature increase in the tropical mesosphere with a maximum value of 22.6 K.

### 3.3. Observations of the MLT Dynamics and Temperature by Meteor Radars and Satellite

We examine the dynamical changes in the MLT region in response to the 2019 SH SSW using the daily zonal and meridional winds from MRs and daily MLS temperatures near the MR stations from DOY 200 to DOY 300 (about 50 days before and after the central date of the warming). Figure 4 shows the daily zonal and meridional winds from Davis, KSS, and TP MR in the altitude range of 70–100 km. Figure 5 shows the day-to-day variations of atmospheric temperature measured by MLS at the altitudes of 80 and 90 km near the MR stations. The central date of the SSW is denoted by the black vertical lines in Figures 4 and 5.

The mesospheric zonal winds observed by MRs at Davis and KSS are overall eastward until DOY around 240. Later, the zonal winds are reversed as the central date (DOY 253) of the 2019 SH SSW approaches. Around the central date, it is interesting that the eastward winds are re-established in the upper mesosphere at both the locations of Davis and KSS. The mesospheric meridional wind at Davis exhibited slow variations over a period of more than 20 days from DOY 220 to 245: Southward wind from DOY 220 to 232 and its change into northward wind before (~20 days) the central date. The mesospheric meridional winds at KSS were roughly out of phase with those at Davis before the central date. Given that the zonal winds are generally eastward until 10 days before the central date, these meridional wind oscillations over more than 20 days and the out-of-phase relation across the two stations, separated by a large longitudinal distance, are

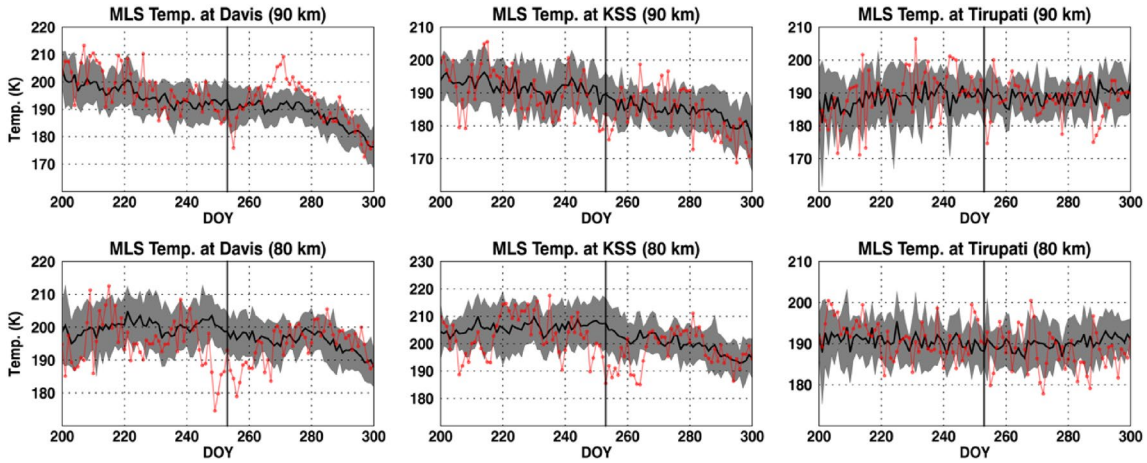


**Figure 5.** The day-to-day variations of neutral atmospheric temperatures at the altitudes of 90 (top) and 80 km (bottom) near the meteor radar (MR) stations. Black lines and the gray areas indicate the climatological mean and its standard deviation. Red lines are the Microwave Limb Sounder temperatures at locations closest to the MR station in 2019. The central date of the sudden stratospheric warming is denoted by the black vertical lines.

likely due to the planetary-scale deformation (stretching or displacement) of the polar night vortex. The mesospheric meridional winds become southward just before the central date at both Davis and KSS. As the southward wind gradually changed to northward (around DOY 260), the eastward winds became weak and turned into westward around 80 km over both stations. These wind changes accompany the cooling at the altitude of 80 km near Davis and KSS (see Figure 5). The present observations during the 2019 SH SSW resemble the earlier SH major SSW. For instance, Hoffmann et al. (2007) showed that there is a large longitudinal discrepancy of meridional winds between similar latitudes near the NH mesopause region. By using the MF radars over the Antarctic region, Dowdy et al. (2004) reported that the magnitude and timing of meridional wind variation were different for each station, but the reversal of zonal wind was relatively consistent between the Antarctic stations.

At the TP station, located in the northern low-latitude region, we noted from Figure 4 that the strong northward winds appeared above the altitude of ~85 km right after the central date and wave-like structures were simultaneously observed in the zonal wind. In this period, Figure 5 indicates that the day-to-day variations of temperatures near the TP region deviate from the climatological mean by more than one standard deviation. Eswaraiah et al. (2019) found wave-like structures in the meridional wind at the altitudes of 75 and 80 km during the 2017 minor NH SSW using the same MR. The meridional wind oscillation occurred right after the peak warming day, and they interpreted it as secondary waves. Their wave-like features are seemingly reminiscent of the zonal winds at TP station after the SSW central date, as shown in Figure 4. In order to investigate the wave activities, we describe the results of a wavelet analysis in the following section.

### 3.4. Wavelet Analysis

The Morlet wavelet analysis (Torrence & Compo, 1998) is adopted to extract the wave activity from the MR zonal wind data. Because the wave amplitude in the meridional wind is much smaller than that in the zonal wind, we only present the wavelet results of the zonal wind. The analysis includes the zonal wind data at the altitudes of 74, 82, 90, and 98 km for each station from DOY 190 to 310, with missing data linearly interpolated. The analysis results are shown for DOY 220–280 in Figure 6, excluding the low confidence periods at both ends.

The characteristics of the wave activity from the Davis MR are remarkably similar to those from the KSS MR except for the altitude of 74 km. Specifically, the quasi 10-day wave (Q10DW) appeared at an altitude of 82, 90, and 98 km above the Davis and KSS stations before the central date of the SSW and reached the maximum amplitude about 10 days before the central date. In the case of Davis Station, the amplitude of Q10DW continued to be strong until ~5 days after the central date of warming. However, in KSS station, the intensity of this wave gradually decreased before the central date. The wave activities at 74 km seem

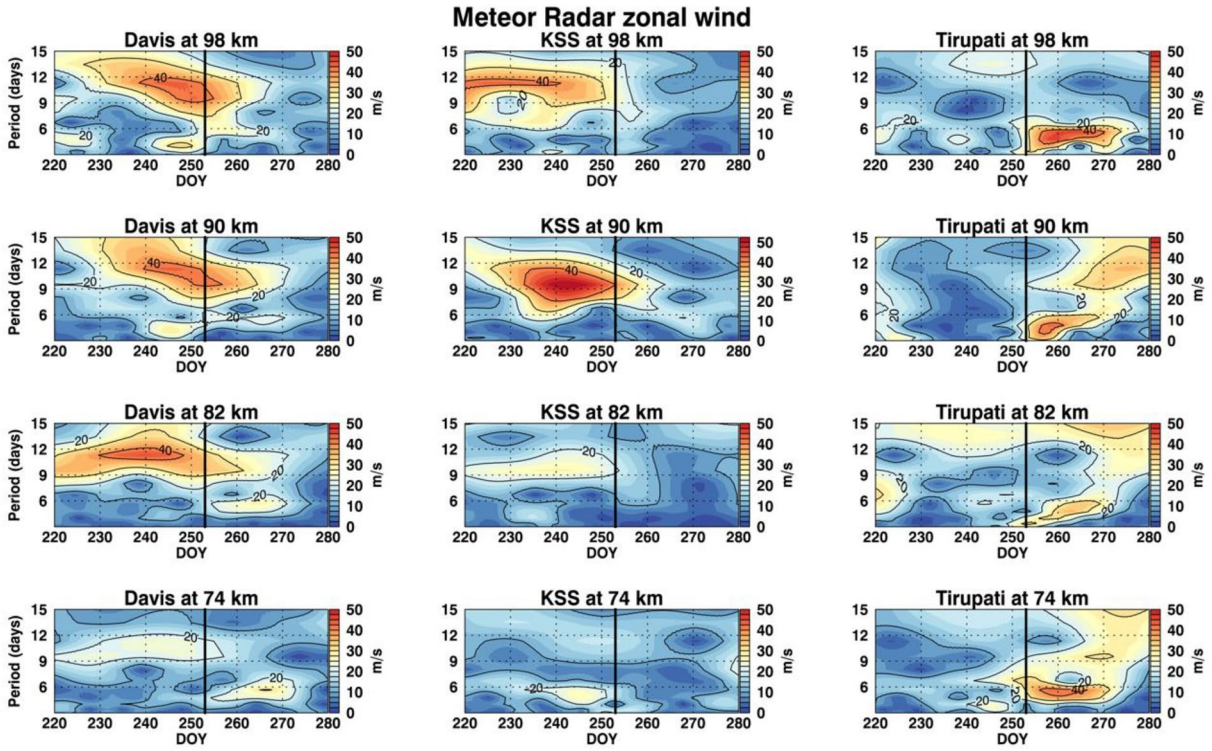


**Figure 6.** The wavelet amplitude spectrum of the daily zonal winds at the altitudes of 98, 90, 82, and 74 km over (left) Davis, (middle) King Sejong Station, and (right) Tirupati. The central date of the 2019 Southern Hemisphere sudden stratospheric warming is denoted by the black vertical lines.

different from each other for the two high-latitude stations. This may be due to the relatively small count of echoes at this altitude, leading to larger uncertainties in the MR winds than at other heights. Normally the meteor peak height is at the altitude of 90 km and the full width at the half maximum of the meteor height distribution is about 12 km in winter (Kam et al., 2019; Lee et al., 2016, 2018).

The appearance of the Q10DW before the SSW has been reported in quite a few studies for the NH. For example, Eswaraiah et al. (2019) observed the Q10DW before the central date of the 2017 NH SSW in the mesospheric meridional winds at the low latitude, and a secondary wave with a period of 2–7 days after the SSW. Matthias et al. (2012) performed a composite analysis of long-period waves using high-latitude MF radar and MR (NH), and showed that the Q10DW dominantly had a westward-propagating component and it accompanied the increasing temperature in the polar stratosphere. Also, Pancheva et al. (2008) reported the appearance of the Q10DW before warming and suggested that the Q10DW originates from the stratosphere and that it can generate zonally symmetric waves by interacting with quasi-stationary PWs.

In the low-latitude TP station during the 2019 SSW (right column of Figure 6), the quasi 6-day wave (Q6DW) turned up after the central date of the warming, but the Q10DW activity was not observed before the central date. The Q6DW appeared at all the altitudes of 74–98 km right after the central date of the 2019 SSW and remained for ~20 days, most prominently at the altitude of 98 km. It is remarkable that the low-latitude station was somehow influenced by the SSW in the Antarctic region through the Q6DW after the warming.

To compare the features of the PW activity as observed in the MRs, we also analyzed the GPH data from Aura/MLS in the MLT region and presented the results in Figure 7. The structures of the amplitude spectrum of the GPHs is similar to those from the MR zonal winds. The Q10DW appeared clearly around the central date of the SSW near Davis Station at the pressure level of 0.001 hPa (~90 km) and 0.05 hPa (~70 km) but not as clear as at 0.01 hPa (~80 km). Over KSS station, the Q10DW is seen at the pressure level of 0.001 and 0.05 hPa before the central date of the warming, but is very weak or absent at 0.01 hPa. Instead, the Q6DW is very strong at the pressure level of 0.01 hPa (~80 km) right after the central date. The Q6DW appeared at the 0.001 and 0.01 hPa near TP station after the central date of the SSW, which is similar to the

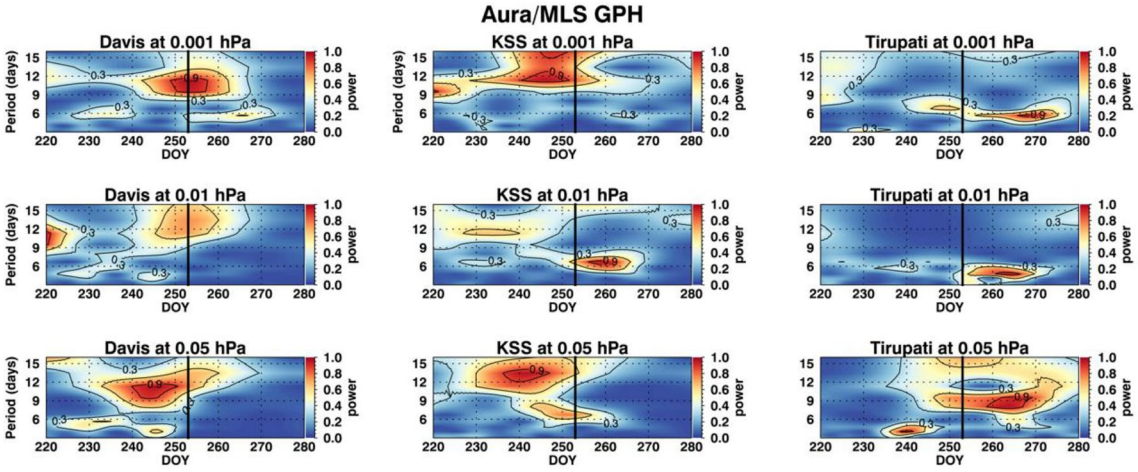


**Figure 7.** The wavelet amplitude spectrum of the daily Microwave Limb Sounder geopotential heights at the pressure levels of (top) 0.001 hPa (~90 km), (middle) 0.01 hPa (~80 km), and (bottom) 0.05 hPa (~70 km) near (left) the Davis, (center) King Sejong Station, and (right) TP meteor radars. The central date of the 2019 Southern Hemisphere sudden stratospheric warming is indicated by the black vertical lines.

ground-based MR observations. In summary, the ground-based MR and satellite observations suggest that the 2019 SH SSW can affect both the high- and low-latitude mesospheric regions through the Q10DW and Q6DW before and after the central date of the SSW, respectively. These planetary wave activities have been reported for the 2019 SH SSW (Eswaraiah et al., 2020; Miyoshi & Yamazaki, 2020; Yamazaki et al., 2020), but their source and propagation have not yet been studied in any concrete way.

### 3.5. Planetary Wave Source and Propagation

The Q10DW and Q6DW activities are expected to be reflected in the MERRA-2 reanalysis data set because the mesospheric flow of MERRA-2 has been improved by assimilating the EOS Aura MLS temperature profiles above 5 hPa since 2005 (Gelaro et al., 2017). However, the MERRA-2 data do not fully include the MLT region, and the Goddard Earth Observing System version 6 (GEOS-6) model used in the production of MERRA-2 employs some ad hoc damping processes such as divergence damping (Fujiwara et al., 2017) and Rayleigh damping in addition to the updated gravity wave drag parameterization (Molod et al., 2012) near the top (0.01 hPa) of the model. Hence, in order to properly understand the potential source of the Q10DW and Q6DW and their propagation to the MLT region, we carry out an SD-WACCM simulation where the stratospheric part of the WACCM is constrained by the MERRA-2 reanalysis data, as described in Section 2. The simulation is done from January 1, 2018 to December 15, 2019. In the analysis of the PW activity and propagation, simulated global winds and temperatures below the altitude of 120 km during a period of DOY 200–280 in 2019 are used.

Figure 8 presents the Hövmoller diagrams of the zonal winds simulated using SD-WACCM and their two-dimensional (zonal wavenumber and period) spectra. Figures 8a and 8b show the result at the high latitude (65°S) and the altitude of 90 km from DOY 226 to 256 (August 14 to September 13; before the SSW). The results demonstrate that the westward propagating 10-day wave with the zonal wavenumber ($s$) = 1 is dominant in the zonal wind. This dominant period is similar to that observed by the high-latitude MRs. The Q6DW observed by the Tirupati MR also appeared in the simulation with a westward propagation and zonal wavenumber 1 (Figures 8c and 8d). In addition, the 6-day variation is also prominent in the zonal wind at the equator and the altitude of 110 km and has a westward propagation with zonal wavenumber 1 (Figures 8e and 8f). It is remarkable that the SD-WACCM reasonably reproduces the Q10DW and Q6DW in the neutral atmosphere in the MLT region unconstrained by the MERRA-2 data before and after the central date of SSW, respectively. The amplitude of the 6-day waves is comparable with those reflected in the equatorial electrojet (EEJ) intensity from Swarm, as reported by Yamazaki et al. (2020). Considering the fact that EEJ is dominated by the variation of neutral wind at this height, the results of SD-WACCM explain the measured EEJ variation reasonably well.

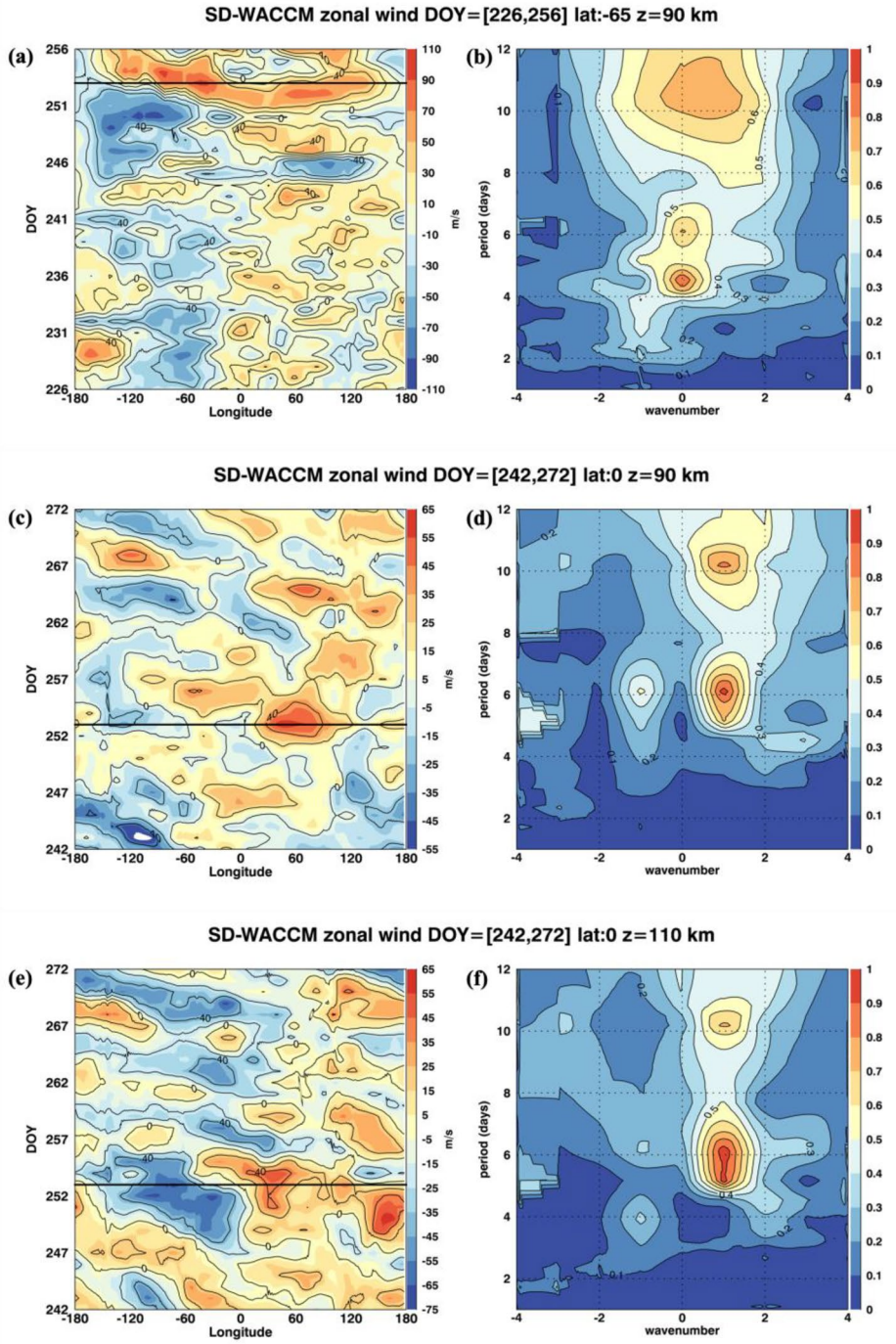


**Figure 8.** Hövmoller diagrams of (left) the Whole Atmosphere Community Climate Model zonal winds and (right) the two-dimensional (zonal wavenumber and period) normalized spectra of the zonal winds (a–b) at the high latitude (65°S) and the altitude of 90 km from DOY 226 to 256 (August 14 to September 13; before the sudden stratospheric warming [SSW]), (c–d) at the equator and the altitude of 90 km during the period of DOY 242–272 (August 30 to September 29) and (e–f) at the equator and the altitude of 110 km for the same time period. Positive wavenumbers denote the westward-propagating waves. The horizontal lines on the Hövmoller diagrams indicate the central date of the 2019 Southern Hemisphere SSW.

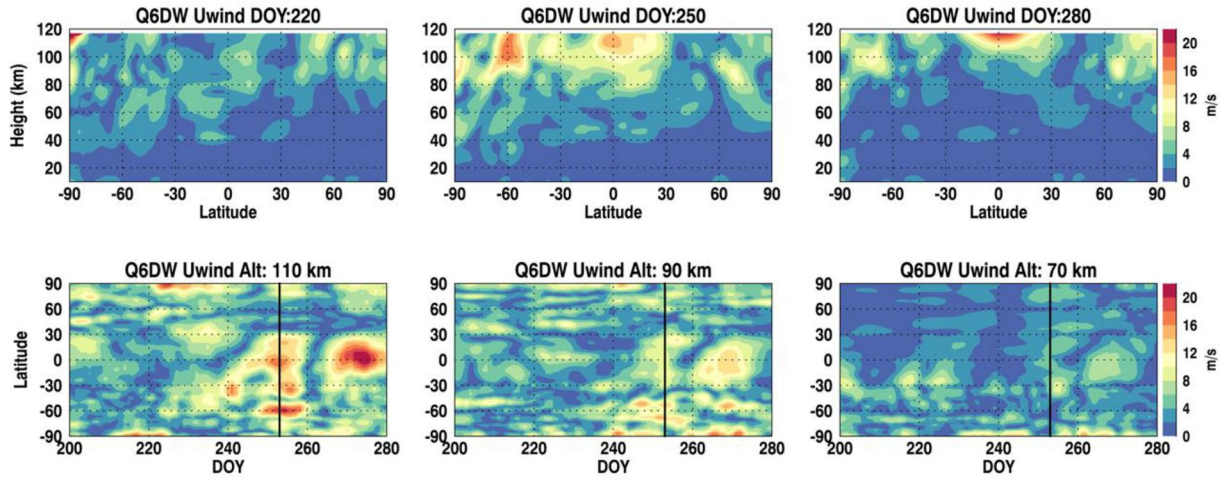


**Figure 9.** Amplitudes of the westward-propagating Q6DW in (top) the latitude-height domain on DOY 220, 250, and 280 and in (bottom) the time-latitude domain at the altitudes of 110, 90, and 70 km.

In this study, we focus on the possible source and propagation of the Q6DW observed in the low-latitude mesospheric region after the central date. The temporal variation of Q6DW amplitudes was derived by using 2D-FFT of the zonal winds on the time versus the longitude plane (such as Figure 8) at each latitude and altitude. We set the time bin of 15 days (center date ±7 days) and selected the westward-propagating zonal wavenumber 1 with a period range of 5–7.5 days. Figure 9 shows the Q6DW amplitudes in the latitude-height domain on DOY 220, 250, and 280 (before the SSW, during the peak of the SSW, and after the SSW, respectively) and in the time-latitude domain at the altitudes of 110, 90, and 70 km.

It is evident from Figure 9 that the Q6DW amplitude is strong in the latitude range of 60°S–30°N at the altitude of 110 km near the central date (DOY 250). At the altitude of 90 km, the amplitude is considerably weaker than that at 110 km but is clearly enhanced in the southern high-latitude region. Near the latitude of 60°S, the amplitude is maximized to 17.6 m/s around the altitude of 100 km on DOY 250. The amplitude also has a local peak of 15.5 m/s around the equator at the altitude of 110 km on the same day. Evidently, the SD-WACCM demonstrates that the SSW invokes the enhancement of the Q6DW activity in the MLT region at both high and low latitudes. By the way, the reappearance of Q6DW around DOY 270 is thought to be of non-SSW origin because the enhancement of Q6DW can occur in the equinoctial month even in non-SSW years (Gan et al., 2018). Given that the SD-WACCM uses the observed information only up to 60 km, it is remarkable that the calculated Q6DW activity is fully consistent with the observed Q6DW enhancement in the mesosphere as described in the previous sections. The calculated Q6DW activity also explains the Q6DW activity reported in the lower ionosphere/thermosphere in the equatorial region (Yamazaki et al., 2020). The enhanced amplitude of Q6DW is comparable to the amplitude of diurnal tide (~20 m/s for September-October 1994 from High Resolution Doppler Interferometer-UARS; Upper Atmosphere Research Satellite) in zonal wind near the equatorial region (Manson et al., 2002).

To investigate the source and propagation of the Q6DW, we used the Eliassen-Palm (EP) flux in spherical coordinates (Andrews et al., 1987) as follows:

$$F^{\phi} = \rho_0 a \cos\phi \left( \overline{u}_z \overline{\theta}_z^{-1} \overline{v'\theta'} - \overline{u'v'} \right)$$

$$F^{z} = \rho_0 a \cos\phi \left[ \left( f - \left( a\cos\phi \right)^{-1} \left( \overline{u}\cos\phi \right)_{\phi} \right) \overline{\theta}_z^{-1} \overline{v'\theta'} - \overline{u'w'} \right]$$

where $F^{\phi}$ and $F^{z}$ are the meridional and vertical component of the EP flux, respectively. The variables, $\rho_0, a$, $\phi$, $f$, and $z$ are the density of air, Earth's radius, latitude, Coriolis parameter, and log-pressure height, respectively; $u$, $\theta$, $v$, and $w$ are the zonal wind, potential temperature, meridional wind, and vertical wind,

respectively. The overbar and prime indicate the zonal mean value and the perturbation due to the Q6DW, respectively, and the subscript means derivative. As proposed by Edmon et al. (1980), the vectors of EP flux are scaled by $(\frac{P_s}{P})^{0.85}[\frac{F^{\phi}}{a\pi}, \frac{F^z}{3\times10^5}]$ to better display the wave flux from the stratosphere to lower thermosphere, where $P_s$ and $P$ are the surface pressure and pressure levels, respectively. The wave energy source and sink region can be verified by the divergence of EP flux ($\nabla \cdot$ F; EPD) and EPD is normalized by $\rho_0 a\cos\phi$.

$$\nabla \cdot \mathrm{F} = \frac{1}{a\cos\phi}\left(F^{\phi}\cos\phi\right)_{\phi} + F^z$$

A positive or negative EPD region indicates the region of source or sink of PW activity. In addition to the EP flux and its divergence, we also computed the meridional gradient of quasi-geostrophic potential vorticity (QGPV) and the square of the refractive index ($n^2$) for the Q6DW as follows:

$$\overline{q}_y = 2\Omega\cos\phi - \left(\frac{\left(\overline{u}\cos\phi\right)_{\phi}}{a\cos\phi}\right)_{\phi} - \frac{a}{\rho_0}\left(\frac{\rho_0 f^2}{N^2}\overline{u}_z\right)_z$$

$$n^2 = \frac{\overline{q}_y}{a\left(\overline{u}-c\right)} - \frac{s^2}{a^2\cos^2\phi} - \frac{f^2}{4N^2H^2}$$

where $\Omega$, $N$, $c$, $s$, and $H$ are the earth's rotation rate, buoyancy frequency, phase speed of the Q6DW, zonal wavenumber, and scale height, respectively. It is expected that the waves cannot propagate in the negative $n^2$ region. The negative $\overline{q}_y$ is a necessary condition for barotropic/baroclinic instability, which depends on the horizontal/vertical curvature of mean flow (Matsuno, 1970).

Figures 10 and 11 show the EPD for the Q6DW overlapped with the regions of $\overline{q}_y < 0$ (green shaded area), $n^2 < 0$ (gray shaded area), and the EP flux vectors on DOY 220 and 250 (before the SSW and about the central date, respectively). The bottom rows of Figures 10 and 11 present the meridional component ($F^{\phi}$) and vertical component ($F^z$) of the EP flux. Before the SSW (Figure 10), the EP flux appeared in the region around 60°S and the altitude range of 40–80 km. However, the flux was blocked by the negative $n^2$ region, and thus the wave could not propagate to the equatorial MLT region. Furthermore, the magnitude of the meridional and vertical component of the EP flux on DOY 220 was relatively weaker than those on DOY 250. On DOY 250, the EP flux again appeared in the high-latitude stratospheric region and was also blocked by the negative $n^2$ region, but it is much stronger than the DOY 220 one. Moreover, the region of negative meridional gradient of QGPV, $\overline{q}_y$, moved down to the stratosphere and mesosphere in the SH high-latitude region. Along with the downward movement of the negative $\overline{q}_y$, the positive divergence of EP flux (reddish area in the upper panel of Figure 11) emerged in the SH high-latitude (60–70°S) mesopause region, which is related to the baroclinic/barotropic instability region. The flux that was generated from the high-latitude mesospheric region can propagate to the equatorial region. The northward component of the EP flux expanded all the way to the NH with an enhanced strength. Thus, we can suggest that the Q6DW observed in the northern tropical mesopause region by the Tirupati MR originated from the SH high-latitude mesopause region near the central date of the 2019 SH SSW. It is remarkable that the observed PW activity in the MLT can be connected from the high-latitude source region all the way to the northern tropical region in the physical model that is constrained only by the reanalysis data in the stratosphere.

## 4. Summary and Conclusion

An unusually strong SSW occurred in the Southern Hemisphere in early September 2019. Based on the MERRA-2 reanalysis data and the WMO's definition of SSW, the 2019 SSW can be classified as a displacement type of minor SSW, but the temperature increase was record-breaking, stronger than the 2002 major SSW.

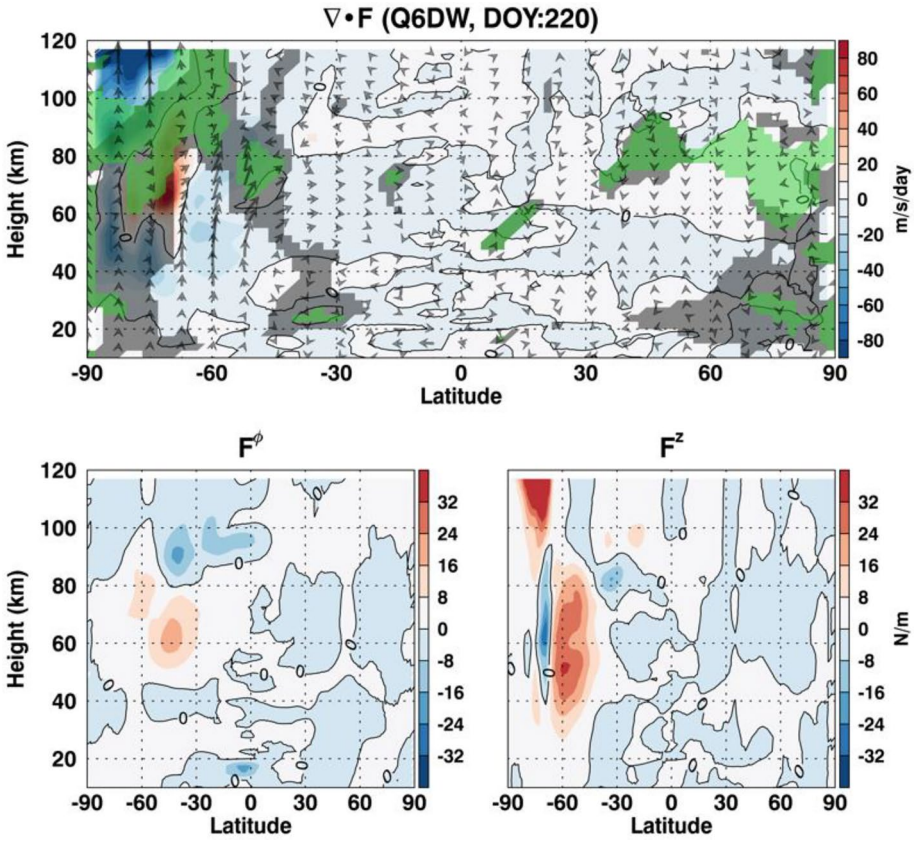


**Figure 10.** (top) The divergence of Eliassen-Palm (EP) flux for the Q6DW along with the region of $\bar{q}_y < 0$ (green shaded area), $n^2 < 0$ (gray shaded area), and the EP flux vector (black vectors). (bottom) The meridional ($F^{\phi}$) and vertical components ($F^{z}$) of the EP flux on DOY 220.

The temperature observations from Aura/MLS show that the zonal mean temperature increased and decreased in the southern polar stratosphere and mesosphere, respectively, before the central date of the 2019 SSW. In addition, the longitudinal asymmetry of the temperatures was observed in the high-latitude stratospheric region, but the asymmetry diminished in the high-latitude mesospheric region. Furthermore, the temperature increase was observed in the tropical mesospheric region.

Horizontal wind observations from two Antarctic MRs (Davis and KSS) indicate that the reversal of eastward winds occurred before the central date of the SSW at mesospheric altitudes and the corresponding meridional winds changed from southward to northward. Quasi 10-day waves (Q10DW) were dominant before the central date in the Davis and KSS MLT region. However, strong wave activity with a period of ~6 days (Q6DW) was detected in the tropical Tirupati MR winds right after the central date. The GPH from Aura/MLS also shows the Q6DW in the MLT region over Tirupati.

To investigate the possible source and propagation of the Q6DW, we utilize the SD-WACCM model constrained by the MERRA-2 reanalysis data. The simulation results clearly indicate that the amplitude of westward-propagating Q6DW was enhanced after the central date of the SSW in the mesospheric region from high to equatorial and even to northern low latitudes. The simulation also shows that the positive divergence of EP flux, which is related to baroclinic/barotropic instability, arose in the SH high-latitude mesospheric region and the EP flux indicates propagation all the way to the NH equatorial mesosphere. Therefore, we suggest that the Q6DW observed by the Tirupati MR and Aura/MLS near the equatorial region originated from the high-latitude mesospheric region. In conclusion, the observation and simulation results clearly indicate that the 2019 SH SSW affected not only the high-latitude MLT region but also the low-latitude MLT region via the Q6DW activity.

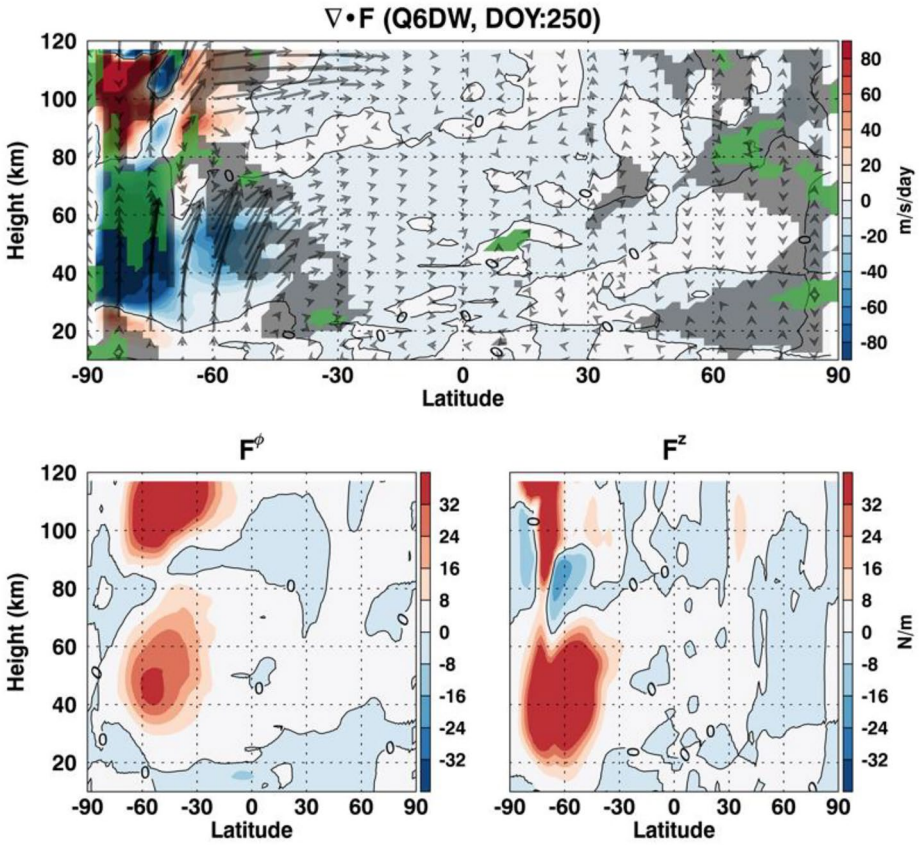


**Figure 11.** Same as Figure 10 but for DOY 250.

## Data Availability Statement

The King Sejong Station meteor radar data are available from https://dx.doi.org/doi:10.22663/KOPRI-KP-DC-00001278.2. The Davis meteor radar data are available from the Australian Antarctic Data Centre at https://data.aad.gov.au/metadata/records/Davis_33MHz_Meteor_Radar. The Tirupati data can be downloaded at http://dx.doi.org/10.17632/3jp89yndnd.1. The Aura/MLS temperature and GPH data are available at http://dx.doi.org/10.5067/Aura/MLS/DATA2021. The MERRA-2 data set can be obtained from https://disc.gsfc.nasa.gov/datasets/M2I6NVANA_5.12.4/summary. WACCM is a component model for the atmosphere in the Community Earth System Model version 2 (CESM2) developed at the National Center for Atmospheric Research (NCAR). The source code is available at https://github.com/ESCOMP/CESM. The atmospheric forcing data for specified dynamics run can be obtained at https://rda.ucar.edu/datasets/ds313.3/index.html

**Acknowledgments**
This work was supported by the Korea Polar Research Institute (PE21020), Incheon, South Korea. Support for the Davis meteor radar data was provided by the Australian Antarctic Program under AAS project 4445. The second author (In-Sun Song) was supported by the Korea Astronomy and Space Science Institute under the R&D program (Project No. 2021-1-850-05) supervised by the Ministry of Science and ICT. We thank Prof. SVB Rao of S.V. University, Tirupati, India for providing the Tirupati Meteor Radar data.

## References

Andrews, D. G., Holton, J. R., & Leovy, C. B. (1987). *Middle atmosphere dynamics*. Academic Press.

Azeem, S. M. I., Talaat, E. R., Sivjee, G. G., Liu, H. L., & Roble, R. G. (2005). Observational study of the 4-day wave in the mesosphere preceding the sudden stratospheric warming events during 1995 and 2002. *Geophysical Research Letters*, *32*(15), 2–5. https://doi.org/10.1029/2005GL023393

Azeem, S. M. I., Talaat, E. R., Sivjee, G. G., & Yee, J.-H. (2010). Mesosphere and lower thermosphere temperature anomalies during the 2002 Antarctic stratospheric warming event. *Annales Geophysicae*, *28*(1), 267–276. https://doi.org/10.5194/angeo-28-267-2010

Bhagavathiammal, G. J., Sathishkumar, S., Sridharan, S., & Gurubaran, S. (2016). Comparison of the dynamical response of low latitude middle atmosphere to the major stratospheric warming events in the Northern and Southern Hemispheres. *Journal of Atmospheric and Solar-Terrestrial Physics*, *146*, 205–214. https://doi.org/10.1016/j.jastp.2016.06.007

Brakebusch, M., Randall, C. E., Kinnison, D. E., Tilmes, S., Santee, M. L., & Manney, G. L. (2013). Evaluation of whole Atmosphere Community Climate Model simulations of ozone during Arctic winter 2004–2005. *Journal of Geophysical Research: Atmospheres*, *118*, 2673–2688. https://doi.org/10.1002/jgrd.50226

Chandran, A., & Collins, R. L. (2014). Stratospheric sudden warming effects on winds and temperature in the middle atmosphere at middle and low latitudes: A study using WACCM. *Annales Geophysicae*, *32*(7), 859–874. https://doi.org/10.5194/angeo-32-859-2014

Chang, L. C., Palo, S. E., & Liu, H.-L. (2009). Short-term variation of thes= 1 nonmigrating semidiurnal tide during the 2002 stratospheric sudden warming. *Journal of Geophysical Research*, *114*(3), 1–13. https://doi.org/10.1029/2008JD010886

Danabasoglu, G., Lamarque, J.-F., Bacmeister, J., Bailey, D. A., DuVivier, A. K., Edwards, J., et al. (2020). The Community Earth System Model Version 2 (CESM2). *Journal of Advances in Modeling Earth Systems*, *12*, e2019MS001916. https://doi.org/10.1029/2019MS001916

Dowdy, A. J., Vincent, R. A., Murphy, D. J., Tsutsumi, M., Riggin, D. M., & Jarvis, M. J. (2004). The large-scale dynamics of the mesosphere-lower thermosphere during the Southern Hemisphere stratospheric warming of 2002. *Geophysical Research Letters*, *31*(14), 3–6. https://doi.org/10.1029/2004GL020282

Dowdy, A. J., Vincent, R. A., Tsutsumi, M., Igarashi, K., Murayama, Y., Singer, W., et al. (2007). Polar mesosphere and lower thermosphere dynamics: 2. Response to sudden stratospheric warmings. *Journal of Geophysical Research*, *112*(17), 1–14. https://doi.org/10.1029/2006JD008127

Edmon, H. J., Hoskins, B. J., & McIntyre, M. E. (1980). Eliassen-Palm cross sections for the troposphere. *Journal of the Atmospheric Sciences*, *37*(12), 2600–2616. https://doi.org/10.1175/1520-0469(1980)037<2600:epcsft>2.0.co;2

Eswaraiah, S., Kim, J. H., Lee, W., Hwang, J., Kumar, K. N., & Kim, Y. H. (2020). Unusual Changes in the Antarctic middle atmosphere during the 2019 warming in the southern hemisphere. *Geophysical Research Letters*, *47*(19), 1–11. https://doi.org/10.1029/2020GL089199

Eswaraiah, S., Kim, Y. H., Hong, J., Kim, J.-H., Ratnam, M. V., Chandran, A., et al. (2016). Mesospheric signatures observed during 2010 minor stratospheric warming at King Sejong Station (62°S, 59°W). *Journal of Atmospheric and Solar-Terrestrial Physics*, *140*, 55–64. https://doi.org/10.1016/j.jastp.2016.02.007

Eswaraiah, S., Kim, Y. H., Lee, J., Ratnam, M. V., & Rao, S. V. B. (2018). Effect of southern hemisphere sudden stratospheric warmings on Antarctica mesospheric tides: First observational study. *Journal of Geophysical Research: Space Physics*, *123*(3), 2127–2140. https://doi.org/10.1002/2017JA024839

Eswaraiah, S., Kim, Y. H., Liu, H., Ratnam, M. V., & Lee, J. (2017). Do minor sudden stratospheric warmings in the Southern Hemisphere (SH) impact coupling between stratosphere and mesosphere-lower thermosphere (MLT) like major warmings? *Earth Planets and Space*, *69*(1), 4–11. https://doi.org/10.1186/s40623-017-0704-5

Eswaraiah, S., Venkat Ratnam, M., Kim, Y. H., Kumar, K. N., Venkata Chalapathi, G., Ramanajaneyulu, L., et al. (2019). Advanced meteor radar observations of mesospheric dynamics during 2017 minor SSW over the tropical region. *Advances in Space Research*, *64*(10), 1940–1947. https://doi.org/10.1016/j.asr.2019.05.039

Eyring, V., Chipperfield, M. P., Giorgetta, M. A., Kinnison, D. E., Matthes, K., Newman, P. A., et al. (2008). Overview of the new CCMval reference and sensitivity simulations in support of upcoming ozone and climate assessments and the planned SPARC CCMVal report. *SPARC Newsletter*, *30*, 20–26.

Eyring, V., Lamarque, J.-F., Hess, P., Arfeuille, F., Bowman, M. P., Chipperfield, K., et al. (2013). Overview of IGAC/SPARC Chemistry-Climate Model Initiative (CCMI) community simulations in support of upcoming ozone and climate assessments. *SPARC Newsletter*, *40*, 48–66.

Fritz, S., & Soules, S. D. (1970). Large-scale temperature changes in the stratosphere observed from Nimbus III. *Journal of the Atmospheric Sciences*, *27*(7), 1091–1097. https://doi.org/10.1175/1520-0469(1970)027<1091:LSTCIT>2.0.CO;2

Fujiwara, M., Wright, J. S., Manney, G. L., Gray, L. J., Anstey, J., Birner, T., et al. (2017). Introduction to the SPARC Reanalysis Intercomparison Project (S-RIP) and overview of the reanalysis systems. *Atmospheric Chemistry and Physics*, *17*(2), 1417–1452. https://doi.org/10.5194/acp-17-1417-20107

Gan, Q., Eastes, R. W., Burns, A. G., Wang, W., Qian, L., Solomon, S. C., et al. (2020). New observations of large-scale waves coupling with the ionosphere made by the GOLD mission: Quasi-16-Day wave signatures in the F-Region OI 135.6-nm nightglow during sudden stratospheric warmings. *Journal of Geophysical Research: Space Physics*, *125*(4), 1–9. https://doi.org/10.1029/2020JA027880

Gan, Q., Oberheide, J., & Pedatella, N. M. (2018). Sources, sinks, and propagation characteristics of the quasi 6-day wave and its impact on the residual mean circulation. *Journal of Geophysical Research - D: Atmospheres*, *123*(17), 9152–9170. https://doi.org/10.1029/2018JD028553

Gelaro, R., McCarty, W., Suárez, M. J., Todling, R., Molod, A., Takacs, L., et al. (2017). The modern-era retrospective analysis for research and applications, version 2 (MERRA-2). *Journal of Climate*, *30*(14), 5419–5454. https://doi.org/10.1175/JCLI-D-16-0758.1

Gettelman, A., Mills, M. J., Kinnison, D. E., Garcia, R. R., Smith, A. K., Marsh, D. R., et al. (2019). The Whole Atmosphere Community Climate Model Version 6 (WACCM6). *Journal of Geophysical Research: Atmospheres*, *124*(23), 12380–12403. https://doi.org/10.1029/2019JD030943

Goncharenko, L. P., Harvey, V. L., Greer, K. R., Zhang, S. R., & Coster, A. J. (2020). Longitudinally dependent low-latitude ionospheric disturbances linked to the Antarctic sudden stratospheric warming of September 2019. *Journal of Geophysical Research: Space Physics*, *125*(8), 1–13. https://doi.org/10.1029/2020JA028199

Guharay, A., & Batista, P. P. (2019). On the variability of tides during a major stratospheric sudden warming in September 2002 at Southern hemispheric extra-tropical latitude. *Advances in Space Research*, *63*(8), 2337–2344. https://doi.org/10.1016/j.asr.2018.12.037

Guharay, A., Batista, P. P., Clemesha, B. R., & Sarkhel, S. (2014). Response of the extratropical middle atmosphere to the September 2002 major stratospheric sudden warming. *Advances in Space Research*, *53*(2), 257–265. https://doi.org/10.1016/j.asr.2013.11.002

Hernandez, G. (2003). Climatology of the upper mesosphere temperature above South Pole (90°S): Mesospheric cooling during 2002. *Geophysical Research Letters*, *30*(10). https://doi.org/10.1029/2003GL016887

Hoffmann, P., Singer, W., Keuer, D., Hocking, W. K., Kunze, M., & Murayama, Y. (2007). Latitudinal and longitudinal variability of mesospheric winds and temperatures during stratospheric warming events. *Journal of Atmospheric and Solar-Terrestrial Physics*, *69*(17–18), 2355–2366. https://doi.org/10.1016/j.jastp.2007.06.010

Holdsworth, D. A., Murphy, D. J., Reid, I. M., & Morris, R. J. (2008). Antarctic meteor observations using the Davis MST and meteor radars. *Advances in Space Research*, *42*(1), 143–154. https://doi.org/10.1016/j.asr.2007.02.037

Hurrell, J. W., Hack, J. J., Shea, D., Caron, J. M., & Rosinski, J. (2008). A new sea surface temperature and sea ice boundary dataset for the Community Atmosphere Model. *Journal of Climate*, *21*(19), 5145–5153.

Kam, H., Kim, Y. H., Mitchell, N. J., Kim, J.-H., & Lee, C. (2019). Evaluation of estimated mesospheric temperatures from 11-year meteor radar datasets of King Sejong Station (62°S, 59°W) and Esrange (68°N, 21°E). *Journal of Atmospheric and Solar-Terrestrial Physics*, *196*(October), 105148. https://doi.org/10.1016/j.jastp.2019.105148

Kim, J.-H., Kim, Y. H., Lee, C.-S., & Jee, G. (2010). Seasonal variation of meteor decay times observed at King Sejong Station (62.22°S, 58.78°W), Antarctica. *Journal of Atmospheric and Solar-Terrestrial Physics*, *72*(11–12), 883–889. https://doi.org/10.1016/j.jastp.2010.05.003

King, J. H., & Papitashvili, N. E. (2005). Solar wind spatial scales in and comparisons of hourly Wind and ACE plasma and magnetic field data. *Journal of Geophysical Research*, *110*, A02104. https://doi.org/10.1029/2004JA010649

Koushik, N., Kumar, K. K., Ramkumar, G., & Subrahmanyam, K. V. (2018). Response of equatorial and low latitude mesosphere lower thermospheric dynamics to the northern hemispheric sudden stratospheric warming events. *Journal of Atmospheric and Solar-Terrestrial Physics*, *169*(December 2017), 66–77. https://doi.org/10.1016/j.jastp.2018.01.021

Krüger, K., Naujokat, B., & Labitzke, K. (2005). The unusual midwinter warming in the Southern Hemisphere stratosphere 2002: A comparison to Northern Hemisphere phenomena. *Journal of the Atmospheric Sciences*, *62*(3), 603–613. https://doi.org/10.1175/JAS-3316.1

Laskar, F. I., McCormack, J. P., Chau, J. L., Pallamraju, D., Hoffmann, P., & Singh, R. P. (2019). Interhemispheric meridional circulation during sudden stratospheric warming. *Journal of Geophysical Research: Space Physics*, *124*(8), 7112–7122. https://doi.org/10.1029/2018JA026424

Lee, C., Jee, G., Kim, J.-H., & Song, I.-S. (2018). Meteor echo height ceiling effect and mesospheric temperature estimation from meteor radar observations. *Annales Geophysicae*, *36*(5), 1267–1274. https://doi.org/10.5194/angeo-36-1267-2018

Lee, C., Kim, J.-H., Jee, G., Lee, W., Song, I.-S., & Kim, Y. H. (2016). New method of estimating temperatures near the mesopause region using meteor radar observations. *Geophysical Research Letters*, *43*(20), 10580–10585. https://doi.org/10.1002/2016GL071082

Livesey, N. J., Read, W. G., Wagner, P. A., Froidevaux, L., Lambert, A., Manney, G. L., et al. (2018). *Earth Observing System (EOS) Aura Microwave Limb Sounder (MLS)*. (Technical Report). NASA Jet Propulsion Laboratory. Retrieved from https://mls.jpl.nasa.gov/data/v4-2_data_quality_document.pdf

Manson, A. H., Luo, Y., & Meek, C. (2002). Global distributions of diurnal and semi-diurnal tides: Observations from HRDI-UARS of the MLT region. *Annales Geophysicae*, *20*(11), 1877–1890. https://doi.org/10.5194/angeo-20-1877-2002

Matsuno, T. (1970). Vertical propagation of stationary planetary waves in the Winter northern hemisphere. *Journal of the Atmospheric Sciences*, 2. https://doi.org/10.1175/1520-0469(1970)027<0871:vpospw>2.0.co

Matsuno, T. (1971). A dynamical model of the stratospheric sudden warming. *Journal of the Atmospheric Sciences*, 2. https://doi.org/10.1175/1520-0469(1971)028<1479:admots>2.0.co

Matthias, V., Hoffmann, P., Manson, A., Meek, C., Stober, G., Brown, P., & Rapp, M. (2013). The impact of planetary waves on the latitudinal displacement of sudden stratospheric warmings. *Annales Geophysicae*, *31*(8), 1397–1415. https://doi.org/10.5194/angeo-31-1397-2013

Matthias, V., Hoffmann, P., Rapp, M., & Baumgarten, G. (2012). Composite analysis of the temporal development of waves in the polar MLT region during stratospheric warmings. *Journal of Atmospheric and Solar-Terrestrial Physics*, *90–91*(1), 86–96. https://doi.org/10.1016/j.jastp.2012.04.004

Mbatha, N., Sivakumar, V., Malinga, S. B., Bencherif, H., & Pillay, S. R. (2010). Study on the impact of sudden stratosphere warming in the upper mesosphere-lower thermosphere regions using satellite and HF radar measurements. *Atmospheric Chemistry and Physics*, *10*(7), 3397–3404. https://doi.org/10.5194/acp-10-3397-2010

Miyoshi, Y., Fujiwara, H., Jin, H., & Shinagawa, H. (2015). Impacts of sudden stratospheric warming on general circulation of the thermosphere. *Journal of Geophysical Research: Space Physics*, *120*(12), 10897–10912. https://doi.org/10.1002/2015JA021894

Miyoshi, Y., & Yamazaki, Y. (2020). Excitation mechanism of ionospheric 6-Day oscillation during the 2019 September sudden stratospheric warming event. *Journal of Geophysical Research: Space Physics*, *125*(9). https://doi.org/10.1029/2020JA028283

Molod, A., Takacs, L., Suarez, M., Bacmeister, J., Song, I.-S., & Eichmann, A. (2012). The GEOS-5 atmospheric general circulation model: Mean climate and development from MERRA to Fortuna(NASA Tech. Rep. NASA/TM-2012-104606, Vol. 28, P. 115). Retrieved from https://gmao.gsfc.nasa.gov/pubs/docs/tm28.pdf

Nakagawa, K. I. & Yamazaki, K. (2006). What kind of stratospheric sudden warming propagates to the troposphere? *Geophysical Research Letters*, *33*, L04801. https://doi.org/10.1029/2005GL024784

Newman, P. A., & Nash, E. R. (2005). The unusual Southern Hemisphere stratosphere winter of 2002. *Journal of the Atmospheric Sciences*, *62*(3), 614–628. https://doi.org/10.1175/JAS-3323.1

Palo, S. E., Forbes, J. M., Zhang, X., Russell, J. M., Mertens, C. J., Mlynczak, M. G., et al. (2005). Planetary wave coupling from the stratosphere to the thermosphere during the 2002 Southern Hemisphere pre-stratwarm period. *Geophysical Research Letters*, *32*(23), 1–5. https://doi.org/10.1029/2005GL024298

Pancheva, D., Mukhtarov, P., Mitchell, N. J., Andonov, B., Merzlyakov, E., Singer, W., et al. (2008). Latitudinal wave coupling of the stratosphere and mesosphere during the major stratospheric warming in 2003/2004. *Annales Geophysicae*, *26*(3), 467–483. https://doi.org/10.5194/angeo-26-467-2008

Pedatella, N., Chau, J., Schmidt, H., Goncharenko, L., Stolle,C., Hocke, K., et al. (2018). How sudden stratospheric warming affects the whole atmosphere. *Eos*, *99*, 6. https://doi.org/10.1029/2018eo092441

Rao, J., Garfinkel, C. I., White, I. P. & Schwartz, C. (2020). The Southern Hemosphere minor sudden stratospheric warming in September 2019 and its predictioins in S2S models. *Journal of Geophysical Research: Atmospheres*, *125*(14), e2020JD032723. https://doi.org/10.1029/2020JD032723

Rao, S. V. B., Eswaraiah, S., Venkat Ratnam, M., Kosalendra, E., Kishore Kumar, K., Sathish Kumar, S., et al. (2014). Advanced meteor radar installed at Tirupati: System details and comparison with different radars. *Journal of Geophysical Research - D: Atmospheres*, *119*(21), 11893–11904. https://doi.org/10.1002/2014JD021781

Reynolds, R. W., Rayner, N. A., Smith, T. M., Stokes, D. C., & Wang, W. (2002). An improved in situ and satellite SST analysis for climate. *Journal of Climate*, *15*, 1609–1625.

Sathishkumar, S., & Sridharan, S. (2009). Planetary and gravity waves in the mesosphere and lower thermosphere region over Tirunelveli (8.7°N, 77.8°E) during stratospheric warming events. *Geophysical Research Letters*, *36*(7). https://doi.org/10.1029/2008GL037081

Schwartz, M. J., Lambert, A., Manney, G. L., Read, W. G., Livesey, N. J., Froidevaux, L., et al. (2008). Validation of the Aura Microwave Limb Sounder temperature and geopotential height measurements. *Journal of Geophysical Research*, *113*(D15), 1–23. https://doi.org/10.1029/2007jd008783

Shepherd, M. G., Wu, D. L., Fedulina, I. N., Gurubaran, S., Russell, J. M., Mlynczak, M. G., & Shepherd, G. G. (2007). Stratospheric warming effects on the tropical mesospheric temperature field. *Journal of Atmospheric and Solar-Terrestrial Physics*, *69*(17–18), 2309–2337. https://doi.org/10.1016/j.jastp.2007.04.009

Siskind, D. E., Coy, L., & Espy, P. (2005). Observations of stratospheric warmings and mesospheric coolings by the TIMED SABER instrument. *Geophysical Research Letters*, *32*(9), 1–4. https://doi.org/10.1029/2005GL022399

Song, B. G., Chun, H. Y., & Song, I. S. (2020). Role of gravity waves in a vortex-split sudden stratospheric warming in January 2009. *Journal of the Atmospheric Sciences*, *77*(10), 3321–3342. https://doi.org/10.1175/JAS-D-20-0039.1

Sridharan, S., Raghunath, K., Sathishkumar, S., & Nath, D. (2010). First results of warm mesospheric temperature over Gadanki (13.5°N, 79.2°E) during the sudden stratospheric warming of 2009. *Journal of Atmospheric and Solar-Terrestrial Physics*, *72*(14–15), 1139–1146. https://doi.org/10.1016/j.jastp.2010.06.003

Torrence, C., & Compo, G. P. (1998). A practical guide to wavelet analysis. *Bulletin of the American Meteorological Society*, *79*(1), 61–78. https://doi.org/10.1175/1520-0477(1998)079<0061:APGTWA>2.0.CO;2

Vineeth, C., Pant, T. K., Kumar, K. K., Ramkumar, G., & Sridharan, R. (2009). Signatures of low latitude-high latitude coupling in the tropical MLT region during sudden stratospheric warming. *Geophysical Research Letters*, *36*(20), 1–5. https://doi.org/10.1029/2009GL040375

Yamazaki, Y., Matthias, V., Miyoshi, Y., Stolle, C., Siddiqui, T., Kervalishvili, G., et al. (2020). September 2019 Antarctic sudden stratospheric warming: Quasi-6-Day wave burst and ionospheric effects. *Geophysical Research Letters*, *47*(1), 1–12. https://doi.org/10.1029/2019GL086577

Younger, J. P., Lee, C. S., Reid, I. M., Vincent, R. A., Kim, Y. H., & Murphy, D. J. (2014). The effects of deionization processes on meteor radar diffusion coefficients below 90 km. *Journal of Geophysical Research - D: Atmospheres*, *119*(16), 10027–10043. https://doi.org/10.1002/2014JD021787